



**Promoting Pt catalysis for CO oxidation via the
Mott–Schottky effect**

Journal:	<i>Nanoscale</i>
Manuscript ID	NR-ART-05-2019-004055.R1
Article Type:	Paper
Date Submitted by the Author:	13-Jun-2019
Complete List of Authors:	<p>Wu, Peiwen; Jiangsu university, School of Chemistry and Chemical Engineering ; Oak Ridge National Laboratory, Chemical Science Division</p> <p>Wu, Zili; Oak Ridge National Laboratory, Chemical Science Division and Center for Nanophase Materials Sciences</p> <p>Mullins, David; Oak Ridge National Laboratory, Chemical Sciences Division</p> <p>Yang, Shize; Oak Ridge National Laboratory, Materials Science Technology Division; Brookhaven National Laboratory,</p> <p>Han, Xue; Virginia Tech, Chemical Engineering</p> <p>Zhang, Yafen; Oak Ridge National Laboratory, Chemical Sciences Division</p> <p>Foo, Guo Shiou; Oak Ridge National Laboratory, Chemical Sciences Division</p> <p>Li, Huaming; Jiangsu University, School of Chemistry and Chemical Engineering</p> <p>Zhu, Wenshuai; Jiangsu University, College of Chemistry and Chemical Engineering; Oak Ridge National Lab,</p> <p>Dai, Sheng; Oak Ridge National Laboratory,</p> <p>Zhu, Huiyuan; Virginia Tech, Department of Chemical Engineering</p>



Journal Name

ARTICLE

Promoting Pt catalysis for CO oxidation via the Mott–Schottky effect

Received 00th January 20xx,
Accepted 00th January 20xx

Peiwen Wu,^{a, b} Zili Wu,^b David R Mullins,^b Shi–Ze Yang,^c Xue Han,^d Yafen Zhang,^b Guo Shiou Foo,^b Huaming Li,^a Wenshuai Zhu,^{a,*} Sheng Dai^{b,*} and Huiyuan Zhu^{b, d, *}

DOI: 10.1039/x0xx00000x

www.rsc.org/

CO oxidation is an important reaction both experimentally and industrially, and its performance is usually dominated by the surface charge state. For example, CO oxidation on platinum (Pt) surface requires a proper charge state for the balance of adsorption and activation of CO and O₂. Here, we present a “Mott–Schottky modulated catalysis” on Pt nanoparticles (NPs) via an electron–donating carbon nitride (CN) support with a tunable Fermi level. We demonstrate that properly–charged Pt presents an excellent catalytic CO oxidation activity, with an initial conversion temperature as low as 25 °C and a total CO conversion below 85 °C. The tunable electronic structure of Pt NPs, which is regulated by the Fermi level of CN, is a key factor in dominating the catalytic performance. This “Mott–Schottky modulated catalysis” concept may be extended to maneuver the charge state on other metal catalysts for targeted catalytic reactions.

Introduction

Low–temperature CO oxidation has attracted increasing attention in the past few years, not only because it is an important probe reaction for the fundamental understanding of the catalyst surface properties and reaction mechanism, but also attributes to its practical applications in emission control and purifying of hydrogen in fuel cells^{1–6}. The low–temperature CO oxidation is especially imperative when it comes to the improvement of heat efficiency for future advanced combustion engines, which requires a total CO conversion under 100 °C^{7–9}. To this end, the supported metal–based catalysts have been extensively investigated with the Pt–group metals being spotlighted^{9–12}. On Pt surfaces, CO oxidation is primarily governed by the adsorption and activation of CO and O₂. For example, the supported Pt catalysts with inert supports (SiO₂, C, Al₂O₃, etc.) adsorb CO strongly, thus blocking the dissociative adsorption of O₂; consequently, the oxidation reaction has to take place above the desorption temperature of CO, and the total conversion temperature is usually higher than 150 °C¹³. This “CO poisoning” is ubiquitous on Pt–group metal surfaces in a broad range of catalytic reactions^{14–16}.

To improve Pt catalysis for CO oxidation at low temperature, necessary strategies should be adopted to weaken the CO adsorption and enhance O₂ adsorption^{17, 18}. Recently, several groups, including ours, have demonstrated that by employing either an electron–donating support, such as hexagonal boron nitride¹⁹ or electron–donating adjacent components^{20, 21}, such as organic ligands^{22–24} or multi–metallic nanoparticles (NPs)^{25–27}, the Pt surface would be negatively charged. Once the Pt surface with the excess negative charge interacts with O₂, it immediately results in a weaker O–O bond and a stronger Pt–O₂ bond, leading to enhanced dissociative adsorption of O₂. Meanwhile, regarding the CO adsorption and activation, the excess negative charge on Pt could be a double–edged sword. On one hand, the increased back donation introduced by the excess charge to antibonding 2π* orbitals of adsorbed CO on the Pt surface would undoubtedly activate CO; however, this excess charge could also reinforce the Pt–CO bond. Previously, the negative charge on Pt has demonstrated a beneficial role during CO oxidation^{19, 28}. Nevertheless, the understanding of this charge effect and how to harness this charge flow to further improve Pt catalysis remains elusive. In this work, we found that the negatively–charged Pt species are not always beneficial to the CO oxidation catalysis. Hence, a critical element in the pursuit of superior CO catalysis on Pt is to maneuver the charge state on the surface, reaching a balance between the adsorption and activation of reactants.

Inspired by the Mott–Schottky effect in solid–state physics, i.e. once a Schottky junction is formed between the metal NP and a semi–conductive support, depending on their relative work functions, a charge flow will be established at the interface to reach a Fermi level equilibrium. In the case of Pt, it holds the highest work function among all metal elements, making it capable of accepting electrons from most of the n–type

^a School of Chemistry and Chemical Engineering; Institute for Energy Research, Jiangsu University, Zhenjiang, 212013, China.

^b Chemical Sciences Division, Oak Ridge National Laboratory, Oak Ridge, TN, 37830, USA.

^c Materials Science and Technology Division, Oak Ridge National Laboratory, Oak Ridge, TN, 37830, USA.

^d Chemical Engineering, Virginia Tech, Blacksburg, VA 24061, USA.

Electronic Supplementary Information (ESI) available: [details of any supplementary information available should be included here]. See DOI: 10.1039/x0xx00000x

semiconductor supports²⁹. With a properly designed Mott-Schottky interface between Pt NPs and the support with a tunable work function, here we demonstrate that the degree of charge transfer to Pt can be adjusted to promote CO catalysis.

Carbon nitride (CN), a fascinating conjugated polymer, bears numerous triazine rings in its structure, making it a natural electron donating species³⁰⁻³². CN also encompasses numerous advantages in practical applications, such as thermal stability, chemical stability, low cost, flexible structure, and an adjustable band gap.³³⁻³⁸ Although most of the applications of CN are in photocatalysis, we believe that the adjustable band gap, through a controllable synthesis process, can open up new avenues for heterogeneous catalysis. By tuning its work function and based on the Mott-Schottky effect, the Fermi level difference between the Pt and CN can be adjusted to a proper degree, making the Pt species properly charged for the targeted catalytic reactions.

To prepare CN with different band gaps, we employed a temperature-controlled synthesis method. Specifically, the CN was synthesized by direct calcination of dicyandiamide (DCD) at different temperatures (600 °C, 650 °C, and 700 °C, respectively) to obtain CN-*n*, where *n* is the heating temperature. Detailed analysis showed that the valence bands (VB) of the CNs are fixed, while the conduction bands (CB) are adjustable, therefore tuning their Fermi levels. The CNs were further employed as functional supports for the assembly of Pt NPs. We found that the electronic structure of Pt NPs can be artificially modified by the CN with different Fermi levels. The CN supported Pt NPs (Pt/CNs) were further investigated in the catalytic CO oxidation reaction. The Pt with a proper negative charge introduced by CN-700 demonstrated superior catalytic performance with an initial conversion at room temperature and a total conversion temperature (T_{100}) lower than 85 °C at a space velocity (SV) of $1667 \text{ L g}^{-1} \text{ Pt h}^{-1}$, one of the best catalytic performances for Pt catalysts on non-redox active supports. Detailed experimental studies confirmed the role of the Mott-Schottky effect in tuning the electronic structure of Pt. *Ex-situ* X-ray photoelectron spectroscopy (XPS) analysis suggested the adsorption and activation of CO and O₂ was on Pt surface instead of on CN support. The role of the CNs was mainly to serve as electronic structural tuning supports. This study provides a new strategy and facile way to modulate the electronic structure of metals via the Mott-Schottky effect for catalytic applications.

Experimental

Materials

Oleylamine (OAM, > 90%), Oleic acid (OAC, > 99%), Octadecene (ODE, > 90%), Platinum 2,4-pentanedionate (Pt(acac)₂, > 99.99%), Iron (0) pentacarbonyl (Fe(CO)₅, > 99.99%), Dicyandiamide (DCD, > 99%), Ethanol (> 99.99%), Hexane (> 99.99%), Isopropanol (> 99%). All chemicals were obtained from Sigma-Aldrich Corporation, USA without further purification.

Preparation of catalysts

Preparation of carbon nitride

Carbon nitride (CN) was prepared as follows: 20 g of DCD was placed in a 50 mL ceramic crucible with a cover. Then, the ceramic crucible was covered by its cover and then tightly by an aluminum foil with two layers. Afterward, the crucible was transferred to a muffle furnace, heated to certain temperatures with a ramping rate of 10 °C min⁻¹, and kept there for another 2 hrs. Then, the muffle furnace was naturally cooled down to room temperature. The very hard solids were carefully taken out of the crucible and ground into a fine powder for further use. The heating temperatures were 600 °C, 650 °C, and 700 °C, and the corresponding CNs were denoted as CN-600, CN-650, and CN-700.

Preparation of 3 nm Pt NPs

The preparation of 3 nm Pt NPs was followed from a previous method³⁹. 0.1 g of Pt(acac)₂, 1 mL of OAM, 1 mL of OAC, and 10 mL of ODE were mixed in a four-neck flask. Then, the mixture was magnetically stirred and heated to 65 °C in N₂ atmosphere for dissolution of Pt(acac)₂. The solution was further heated to 180 °C with a ramping rate of 6 °C min⁻¹. When the temperature reached 180 °C, 0.1 mL of Fe(CO)₅ stock solution (0.1 mL of Fe(CO)₅ in 1 mL of hexane) was injected to the solution. Subsequently, the flask was heated to 200 °C and kept for another 1 hr. After the reaction, the mixture was naturally cooled down to room temperature by removing the heat source. Then, 30 mL of isopropanol was added to the mixture and centrifuged with a speed of 8000 rpm for 10 min. The NPs were further re-dispersed in 10 mL of hexane and then washed by ethanol. Finally, the Pt NPs were dispersed in 10 mL of hexane for further use.

Preparation of Pt/CN

The CN supported Pt NPs (Pt/CN) were prepared as follows: 0.1 g of Pt NPs was dispersed in 20 mL of hexane, and 1 g of CN was dispersed in 20 mL ethanol. Then, the Pt NPs solution was added to the CN dispersion dropwise under sonication. The mixed solution was further ultrasonically treated for 2 hrs, and then magnetically stirred overnight at room temperature. Then, the mixture was centrifuged with a speed of 8000 rpm for 20 min and washed by 30 mL of mixed ethanol and hexane (volume ratio is 1: 1) for 3 times each. The samples were denoted as Pt/CN-600, Pt/CN-650, and Pt/CN-700, depending on the preparation temperature of CN. The Pt loading amounts for Pt/CN-600, Pt/CN-650, and Pt/CN-700 were determined by inductively coupled plasma atomic emission spectrometer (ICP-AES) to be 1.21%, 1.20%, and 1.21%, respectively.

Preparation of Pt/SiO₂ and Pt/TiO₂

The preparation processes for Pt/SiO₂ and Pt/TiO₂ are similar to that of Pt/CN by replacing CN with SiO₂ or TiO₂. The accurate Pt loadings for Pt/SiO₂ and Pt/TiO₂ were found to be 1.19% and 1.20% respectively.

Characterizations

Scanning Transmission Electron Microscopy (STEM), High resolution STEM (HR-STEM), and Electron energy loss spectroscopy (EELS) were performed on a Nion Ultra STEM 100 (operated at 100kV). EELS spectra were collected on a high

resolution Gatan-Enfina ER with a probe size of 1.3 Å. X-ray diffraction (XRD) measurements were performed on a PANalytical X'Pert Pro MPD diffractometer using an X'Celerator RTMS detector. *In situ* Diffuse Reflectance Infrared Fourier Transform Spectroscopy (*In situ* DRIFT) measurements were performed on a Nicolet 6700 Fourier Transform Infrared Spectrometer (FT-IR) spectrometer with an MCT detector cooled by liquid nitrogen. All the spectra were scanned for 32 times with a resolution of 4 cm⁻¹. During the testing process, the samples were initially placed in a porous ceramic cup and inserted into an *in-situ* chamber (HC-900, Pike Technologies), and the *in-situ* DRIFT spectra of the samples were taken at different times. Ultraviolet-Visible Diffuse-Reflectance Spectra (UV-Vis DRS) were determined by a Shimadzu UV-2450 spectrophotometer, which is equipped with a spherical diffuse reflectance accessory in the range of 200–800 nm. XPS data were collected using a PHI 3056 spectrometer with an Al anode source operated at 15 kV and an applied power of 350 W with samples mounted on Al foil. ICP was carried out on a VISTA-MPX ICP spectrometer from Varian company. Elemental analysis was performed by a FLASH1112A Element analyzer from Italy EA company. For the tests of *ex-situ* XPS characterization, the Pt/CN-700 catalyst was placed in a reaction chamber. Then a mixed gas of 1 vol.% CO and 99 vol.% air was purged and further kept for another 30 min under 25 °C. Then the treated sample was directly transferred to the XPS analysis chamber avoiding the contact with air to record the XPS spectra.

General procedure for CO oxidation evaluation

The CO oxidation test was conducted in a temperature-controlled microreactor (Altamira AMI 200) equipped with an on-line gas chromatograph. 30 mg of catalyst was placed in the U-shape quartz tube, and both inlets were covered by glass wool. Then, the quartz tube was treated at 200 °C in the air for 1 hr for both catalyst activation and O₂ adsorption. Afterward, a mixed gas, consisting of CO (1.0 vol %) and 99.0 vol% dry air, flowed over the catalyst with a flow rate of 10 mL min⁻¹. The effluent was analyzed by a GC with a thermal conductivity detector (TCD) detector. For the kinetic measurements, the amount of catalyst was reduced to 5 mg to ensure the CO conversions were lower than 15%. The CO conversion was averaged at 10, 20, 30, and 40 min to calculate the reaction rate. The reaction rate (*r*) was calculated by Equation (1).

$$r = \text{CO conversion rate} \times [\text{CO}]_{\text{in}} / n(\text{Pt}) \quad (1)$$

where the CO conversion rate stands for the converted percentage of CO after the CO oxidation reaction, $[\text{CO}]_{\text{in}}$ is the total molar flow of CO per second, and $n(\text{Pt})$ stands for total moles of Pt atoms.

Results and Discussion

Detailed morphologies of the Pt/CNs were investigated by STEM. As shown in Figure 1a, S1 and S2, the STEM high angle annular dark field (HAADF) images of the samples showed that the Pt NPs are uniformly dispersed on the surface of CNs

without aggregation. This dispersion behavior in the high angle annular bright field (HAABF) STEM image in Figure 1b showed that the Pt NPs are located not only at the edges but also spread over the bulk phase of CNs. This dispersion behavior can be attributed to the existence of triazine rings in the CN structure. Each triazine ring is highly electron rich, leading to a favorable interaction with Pt NPs. HR-STEM was carried out on Pt/CN-700. The HR-STEM image of Pt NPs showed a lattice distance of ~0.23 nm (Fig. 1c), which is in accordance of the lattice distance of (111) lattice for Pt. Meanwhile, as shown in Fig. 1d, the HR-STEM characterization of CN presents a lattice distance of ~0.34 nm, corresponding to the (002) plane of graphitic phase carbon nitride. To further analyze the carbon nitride, EELS of Pt/CN-700 was also performed and shown in Fig. S3. Both the transitions 1s→π* and 1s→σ* can be clearly detected in the carbon K edge and nitrogen K-edge. In addition, the relative intensities of the two peaks demonstrate that the prepared CN consists of sp² hybridized carbon and nitrogen, confirming the formation of graphitic CN phase³⁵.

To further characterize the catalysts, a series of spectral experiments were performed. In Fig. S4, the X-ray Diffraction (XRD) patterns of the final products clearly demonstrate the characteristic peaks for graphene-like carbon nitride. Meanwhile, when the CNs were employed as supports in the preparation of Pt/CN-*n*, CN characteristic peaks were retained (Fig. S5), indicating the stability of CN during the assembly process. In Fig. S5, the additional peaks can be assigned to the Pt face-centered cubic (fcc) phase on CN. The broad Pt peaks indicate Pt NPs remain in their original crystalline sizes without aggregation after assembly on CN. The FT-IR spectra in Fig. S6 and S7 further confirmed the formation of a carbon nitride phase with characteristic peaks at 802 and 888 cm⁻¹ for the breathing mode of tri-s-triazine units and a group of peaks in the range of 1200 cm⁻¹ to 1700 cm⁻¹ for the typical C-N heterocycle stretching³⁰, proving our method is an effective way to produce CN. It is worth mentioning that compared to pure CNs in Fig. S6, no additional peaks were detected in Pt/CNs (Fig. S7), indicating that the surfactants on the Pt NPs' surfaces have been totally removed during the assembly and surface activation process, leaving a clean Pt surface for the following catalytic study.

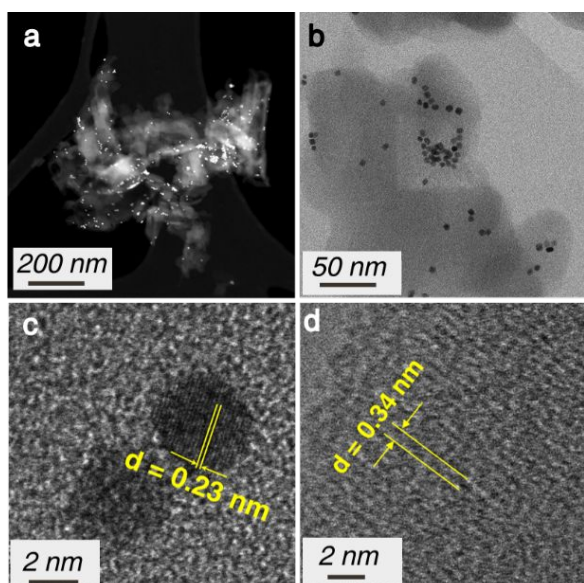


Fig. 1. Characterizations of Pt/CN-700 catalyst. (a) HAADF STEM image of Pt/CN-700; (b) HAADF STEM image of Pt/CN-700; (c) HR-STEM image of Pt in Pt/CN-700, (d) HR-STEM image of CN in Pt/CN-700.

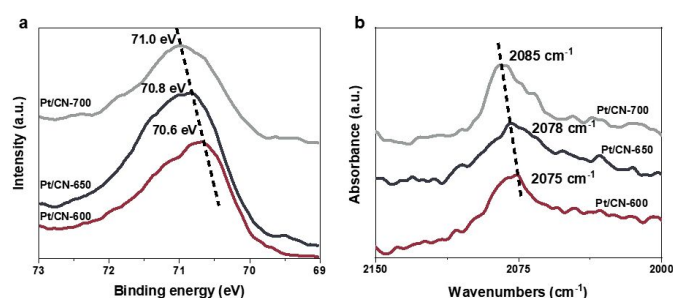


Fig. 2 Mott-Schottky effect on regulating the electronic structure of Pt/CNs. (a) Pt 4f core-level XPS spectra; (b) *in situ* DRIFTS of CO adsorption; the analysis temperature in Fig. 2b is 25 °C, and features from gas phase CO have been subtracted.

To clarify how the Mott-Schottky effect regulates the electronic structures of Pt NPs in Pt/CNs, additional characterizations were carried out. For comparisons, a covalent and inert SiO₂ support without a significant charge transfer to Pt was employed. As shown in the XPS in Fig. S8, the results verified the chemical composition and structure of Pt/CNs. Regarding the Pt4f core-level XPS spectra (Fig. 2a), the Pt 4f_{7/2} peak from Pt/SiO₂ is at 71.4 eV (Fig. S9), while the Pt 4f_{7/2} peaks from the Pt/CNs range from 70.6 to 71.0 eV (Fig. 2a). This indicated that the Pt NPs on CN were more negatively charged than the Pt/SiO₂. Meanwhile, the Pt 4f_{7/2} binding energy for the Pt/CNs increases as the CN preparation temperature increases. The results suggest that the Pt NPs on CNs are negatively charged, and the degree of negative charge decreases with the increasing support preparation temperature. This result was further confirmed by *in situ* DRIFTS following CO adsorption. As shown in Fig. 2b, the linearly adsorbed CO on Pt NPs showed a clear blueshift (from 2076 to 2085 cm⁻¹) with the increasing CN preparation temperature. Since the NPs in all Pt/CNs held the same sizes and similar loading, such a shift is representative of a less

negatively charged Pt surface on CN-700 compared to Pt supported on CN prepared at a lower temperature¹⁹.

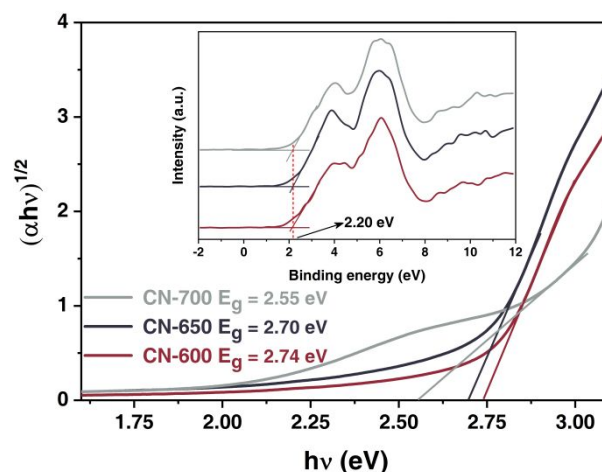


Fig. 3 Band gaps of CNs from UV-Vis DRS spectra. Inset in Fig. 3a is the measured valence band positions of CNs.

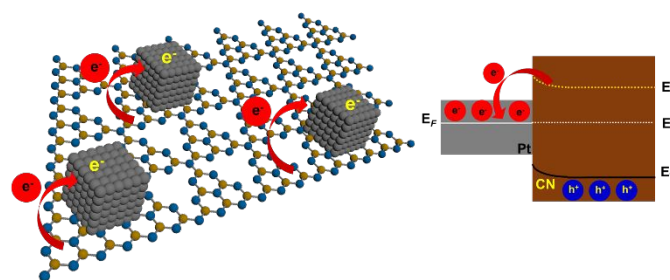


Fig. 4 Scheme illustration of Mott-Schottky effect between Pt NPs and CNs.

In solid-state physics, charge transfer is often detected at the interface of the heterojunction with different Fermi levels, i.e. the electrons flow from the component with a higher Fermi level to the one with a lower Fermi level to reach an equilibrium^{40, 41}. Pt holds the highest work function (lowest Fermi level) among metal elements²⁹, while the CN is a typical n-type semiconductor whose Fermi level is close to its conduction band (CB). The difference between the work functions of Pt and CN induces the formation of a Schottky barrier between Pt NPs and CNs. Furthermore, such difference of Fermi level leads to the bending of energy bands and electrons transfer from CN to Pt to reach equilibrium²⁹. The charge transfer between Pt NPs and CN would produce hot electrons in the Schottky heterojunction, which are in favor of the activation of O for a boosted catalysis^{42, 43}.

In our case, the various degrees of charge transfer from CN to Pt mainly originates from the different properties of the prepared CNs. Elemental analysis of the CNs in Fig. S10 showed that the higher preparation temperature gives rise to a lower nitrogen content, which is related to the band gap of CNs³². We should note here that based on the previous report, no Fermi level pinning would be formed between the Pt NPs and CN supports²⁹. The calculations from Fig. 3a confirmed that the band gaps, obtained from ultraviolet-visible diffuse reflection spectra (UV-Vis DRS), for CN-600, CN-650 and

CN-700 were 2.74, 2.70 and 2.55 eV, respectively. In addition, their valence bands (VB) were determined by XPS valence band spectra and shown in the inset of Fig. 3a, indicating that the VBs were all located at 2.20 eV. The results demonstrate that the preparation temperature of CNs controls their CBs, thereby, modifying the location of Fermi level^{32, 44} and consequently regulating the degree of charge transfer from CNs to Pt.

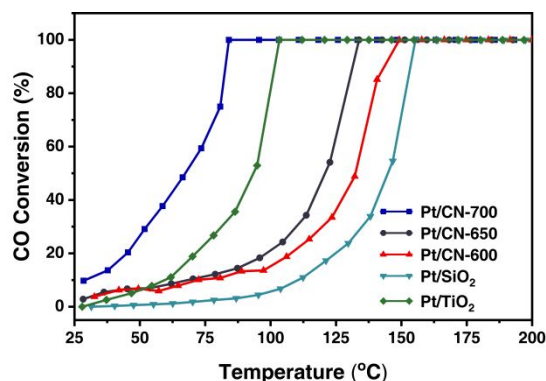


Fig. 5 The CO oxidation activities of Pt/CNs, Pt/TiO₂ and Pt/SiO₂.

To visually illustrate the Mott-Schottky effect on the charge transfer between CN and Pt NPs, a scheme was proposed in Fig. 4. As shown in Fig. 4, the CN prepared at all temperatures has a higher work function than that of Pt, indicating that Pt can accept electrons from CN until their Fermi levels reach equilibrium. For the CN-600, CN-650, CN-700, a narrower band gap represents a lower work function, reducing the difference in Fermi levels between CN and Pt, resulting in less charge transfer to Pt in the sequence of CN-600 > CN-650 > CN-700. The high-resolution XPS peaks of Pt (Fig. 2a) and *in situ* DRIFTS of CO adsorption (Fig. 2b) indicate the negatively-charged degree of Pt NPs on CNs is in the order of Pt/CN-600 > Pt/CN-650 > Pt/CN-700, in favor of the controllable charge transfer over the Mott-Schottky heterojunction at the interface of Pt and CN. Collectively, our results show that the Pt NPs on carbon nitride can be controllably charged by controlling the pyrolysis temperature of the CNs.

All samples with a similar Pt loading amount (~1.20 wt.%) were evaluated by CO oxidation as a probe reaction with an SV of 1667 L g⁻¹ Pt h⁻¹ to investigate their catalytic performance. As shown in Fig. 5, the Pt/CN-700 showed the best catalytic performance with an initial conversion temperature as low as ~25 °C, lower than that of most platinum-based catalysts on non-redox-active supports¹⁹. Meanwhile, the total conversion starts at a reaction temperature lower than 85 °C, which is much lower than Pt on other inert supports and comparable to the redox-active support TiO₂ (Fig. 4). While for other samples, although the initial conversion temperatures for Pt/CN-650, Pt/CN-600 are lower than 30 °C, their T₁₀₀ increased to 135 °C and 145 °C, respectively. The apparent activation energies (E_a) for Pt/CN-700, Pt/CN-650, and Pt/CN-600 were calculated to be 27.1, 41.8, and 47.6 kJ mol⁻¹ (Fig. 6), respectively, indicating Pt NPs on CN-700 holds the

lowest reaction barrier among the prepared samples. The T₁₀₀ for Pt/SiO₂ (155 °C) was higher than those of the Pt/CNs. Additionally, the E_a for Pt/SiO₂ was 60.8 kJ mol⁻¹ (Fig. 5), also much higher than those for Pt NPs on CN.

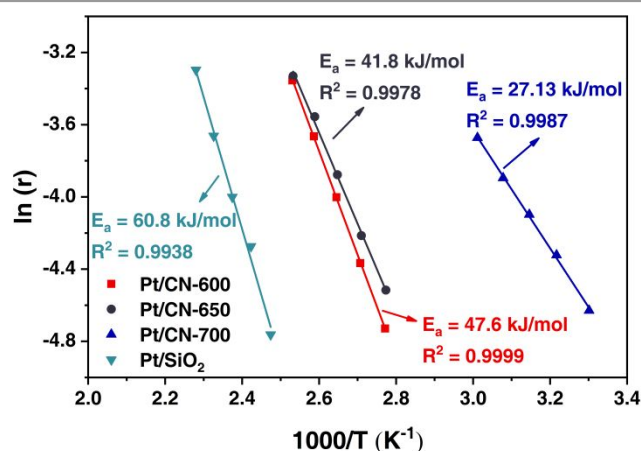


Fig. 6 The calculated apparent activation energies for different samples. The catalysts amounts were reduced to 5 mg to make the CO conversion rate lower than 15%, mixed gas flow rate 10 ml min⁻¹.

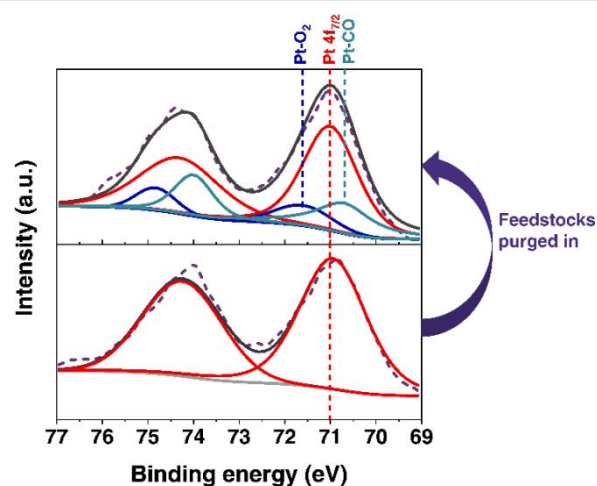


Fig. 7 The *ex-situ* Pt 4f core-level XPS spectra of Pt/CN-700.

To probe the active sites of Pt/CN-700, an *ex-situ* XPS characterization was carried out. The spectra were collected by placing the Pt/CN-700 in the reaction chamber and treating it with a mixed gas of 1 vol.% CO and 99 vol.% air for 30 min at room temperature. Afterward, the sample was directly transferred to the analysis chamber avoiding contact air to record the XPS spectra (Fig. 7 and Fig. S11). No noticeable change was detected in the C1s and N1s spectra in Fig. S11, indicating that when the catalyst contacted with feedstocks; there were no significant interactions between reactants and CN. As shown in Fig. 7, the Pt 4f_{5/2} and Pt 4f_{7/2} peaks, corresponding to only a single state of metallic Pt, were detected prior to gas treatment. Following the gas exposure, another two sets of peaks, whose Pt 4f_{7/2} peaks were located near 71.6 eV and 70.7 eV, were detected. These may be attributed to interactions between Pt NPs and O₂, Pt NPs and CO, respectively^{45,46}. Although Pt-CO is generally observed on

the single crystal Pt surface, a few recent works found that Pt-CO can be also detected on non-single-crystal Pt NPs during CO oxidation processes⁴⁷⁻⁴⁹. This result indicates that the Pt NPs functioned as active sites for activation of CO and O₂ molecules, and the CN worked as the electron tuning support. Taken cumulatively, Pt NPs with charge transfer from CNs can effectively adsorb O₂ molecules, favoring CO and O₂ activation, exemplified by the promoted catalysis on Pt/CN-700. However, this excess charge on Pt does not continuously improve catalysis. As the extraneous electrons on Pt increase, the back donation from 5d orbital to 2π* of the CO molecule strengthens, potentially leading to a stronger CO adsorption, counterbalancing the positive effect on O₂ adsorption and activation, evidenced by the lower performance of more negatively-charged Pt/CN-600 and Pt/CN-650.

The stability test of the best-performing catalyst, Pt/CN-700, was carried out in a time-on-stream experiment in at 30 °C, 45 °C, and 65 °C respectively for 10 hrs, at 100 °C for 30 hrs, and was shown in Fig. 8. The result illustrates that Pt/CN-700 showed stable CO catalytic conversions of 10%, 20% and 50% at 30 °C, 45 °C, and 65 °C respectively for 10 hrs. Additionally, the total CO conversion was maintained at 100 °C after 32 hrs.

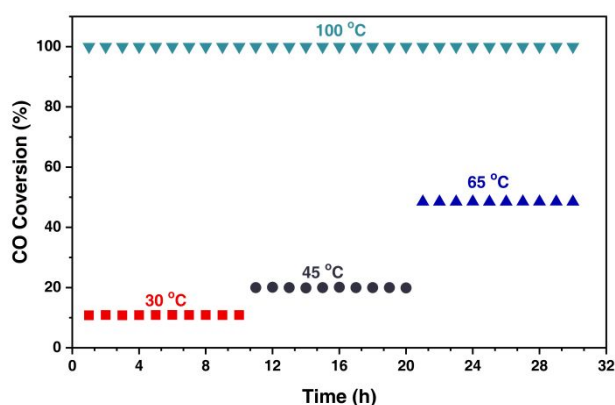


Fig. 8. The stability tests of Pt/CN-700 under different reaction temperatures.

Conclusions

In conclusion, we demonstrate a “Mott-Schottky modulated catalysis” scenario, exemplified by CO oxidation catalysis on Pt. Different synthesis temperatures endow CNs with tunable Fermi levels. Once acting as an electron-tuning support, the CN can properly adjust the electronic structure of Pt via the Mott-Schottky effect. On Pt/CN-700, a balance between reactant adsorption and activation could be obtained. Such properly-charged Pt surface demonstrated a remarkable CO oxidation catalysis with an initial conversion at room temperature and a total conversion temperature < 85 °C at a SV of 1667 Lg⁻¹Pt h⁻¹. This work provides a general strategy for tuning metal electronic structure via the Mott-Schottky effect for enhanced catalytic performance.

Conflicts of interest

There are no conflicts to declare.

Acknowledgements

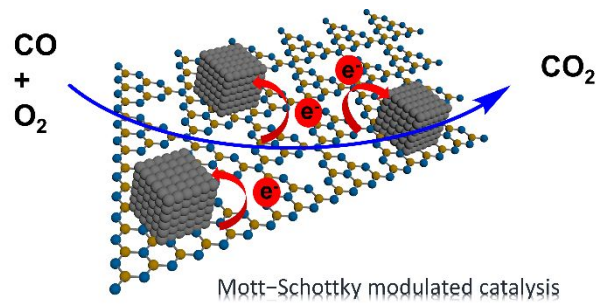
This work was supported by the US Department of Energy, Office of Science, Office of Basic Energy Sciences, Chemical Sciences, Geosciences and Biosciences Division. P.W. W., W.S. Z. and H.M.L. are grateful to the financial support from the National Nature Science Foundation of China (Nos. 21576122, 21722604). P. W. W. is grateful to the China Postdoctoral Science Foundation (2019M651743). The electron microscopy at ORNL (S.Z.Y.) was supported in part by the U.S. Department of Energy, Office of Science, Basic Energy Sciences, Materials Science and Engineering Division and through a user proposal supported by ORNL’s Center for Nanophase Materials Sciences, which is a DOE Office of Science User Facility.

Notes and references

‡ Supplementary material related to this article can be found in the online version

1. J. Saavedra, H. A. Doan, C. J. Pursell, L. C. Grabow and B. D. Chandler, *Science*, 2014, **345**, 1599-1602.
2. K. Ding, A. Gulec, A. M. Johnson, N. M. Schweitzer, G. D. Stucky, L. D. Marks and P. C. Stair, *Science*, 2015, **350**, 189-192.
3. M. Haruta, *Nature*, 2005, **437**, 1098-1099.
4. X.-m. Zhang, Y.-Q. Deng, P. Tian, H.-h. Shang, J. Xu and Y.-F. Han, *Appl. Catal. B Environ.*, 2016, **191**, 179-191.
5. C. Wang, C. Wen, J. Lauterbach and E. Sasmaz, *Appl. Catal. B Environ.*, 2017, **206**, 1-8.
6. H. Guan, J. Lin, L. Li, X. Wang and T. Zhang, *Appl. Catal. B Environ.*, 2016, **184**, 299-308.
7. J. Jones, H. Xiong, A. T. DeLaRiva, E. J. Peterson, P. Hien, S. R. Challa, G. Qi, S. Oh, M. H. Wiebenga, X. I. P. Hernandez, Y. Wang and A. K. Datye, *Science*, 2016, **353**, 150-154.
8. L. Nie, D. Mei, H. Xiong, B. Peng, Z. Ken, X. I. P. Hernandez, A. DeLaRiva, M. Wang, M. H. Engelhard, L. Kovarik, A. K. Datye and Y. Wang, *Science*, 2017, **358**, 1419-+.
9. D. Miller, H. S. Casalongue, H. Bluhm, H. Ogasawara, A. Nilsson and S. Kaya, *J. Am. Chem. Soc.*, 2014, **136**, 6340-6347.
10. S. Bonanni, K. Ait-Mansour, W. Harbich and H. Brune, *J. Am. Chem. Soc.*, 2014, **136**, 8702-8707.
11. L. Tao, S. Dou, Z. Ma and S. Wang, *Electrochim. Acta*, 2015, **157**, 46-53.
12. S. Wang, X. Wang and S. P. Jiang, *Phys. Chem. Chem. Phys.*, 2011, **13**, 6883-6891.
13. B. Qiao, A. Wang, X. Yang, L. F. Allard, Z. Jiang, Y. Cui, J. Liu, J. Li and T. Zhang, *Nat. Chem.*, 2011, **3**, 634-641.
14. J. Liu, F. R. Lucci, M. Yang, S. Lee, M. D. Marcinkowski, A. J. Therrien, C. T. Williams, E. C. H. Sykes and M. Flytzani-Stephanopoulos, *J. Am. Chem. Soc.*, 2016, **138**, 6396-6399.
15. M. J. Lee, J. S. Kang, Y. S. Kang, D. Y. Chung, H. Shin, C.-Y. Ahn, S. Park, M.-J. Kim, S. Kim, K.-S. Lee and Y.-E. Sung, *ACS Catal.*, 2016, **6**, 2398-2407.
16. P. Ferrari, L. M. Molina, V. E. Kaydashev, J. A. Alonso, P. Lievens and E. Janssens, *Angew. Chem. Int. Ed.*, 2016, **55**, 11059-11063.
17. A. D. Allian, K. Takanebe, K. L. Fudjara, X. Hao, T. J. Truex,

- J. Cai, C. Buda, M. Neurock and E. Iglesia, *J. Am. Chem. Soc.*, 2011, **133**, 4498-4517.
18. W. D. Michalak, J. M. Krier, S. Alayoglu, J.-Y. Shin, K. An, K. Komvopoulos, Z. Liu and G. A. Somorjai, *J. Catal.*, 2014, **312**, 17-25.
19. W. Zhu, Z. Wu, G. S. Foo, X. Gao, M. Zhou, B. Liu, G. M. Veith, P. Wu, K. L. Browning, H. N. Lee, H. Li, S. Dai and H. Zhu, *Nat Commun*, 2017, **8**.
20. G. Pacchioni and H. Freund, *Chem. Rev.*, 2013, **113**, 4035-4072.
21. H.-J. Freund and G. Pacchioni, *Chem. Soc. Rev.*, 2008, **37**, 2224-2242.
22. G. Chen, C. Xu, X. Huang, J. Ye, L. Gu, G. Li, Z. Tang, B. Wu, H. Yang, Z. Zhao, Z. Zhou, G. Fu and N. Zheng, *Nat. Mater.*, 2016, **15**, 564-569.
23. L. Altmann, S. Kunz and M. Baeumer, *J. Phys. Chem. C*, 2014, **118**, 8925-8932.
24. I. Schrader, J. Warneke, J. Backenkoehler and S. Kunz, *J. Am. Chem. Soc.*, 2015, **137**, 905-912.
25. K. Jiang, D. Zhao, S. Guo, X. Zhang, X. Zhu, J. Guo, G. Lu and X. Huang, *Sci. Adv.*, 2017, **3**.
26. D. C. Upham, V. Agarwal, A. Khechfe, Z. R. Snodgrass, M. J. Gordon, H. Metiu and E. W. McFarland, *Science*, 2017, **358**, 917-920.
27. V. R. Stamenkovic, F. Ben, M. Bongjin Simon, W. Guofeng, P. N. Ross, C. A. Lucas and N. M. Markovi?, *Science*, 2007, **315**, 493-497.
28. Y. P. G. Chua, G. T. K. K. Gunasooriya, M. Saeys and E. G. Seebauer, *J. Catal.*, 2014, **311**, 306-313.
29. X.-H. Li and M. Antonietti, *Chem. Soc. Rev.*, 2013, **42**, 6593-6604.
30. Y. Wang, J. Yao, H. Li, D. Su and M. Antonietti, *J. Am. Chem. Soc.*, 2011, **133**, 2362-2365.
31. K. Schwinghammer, M. B. Mesch, V. Duppel, C. Ziegler, J. Senker and B. V. Lotsch, *J. Am. Chem. Soc.*, 2014, **136**, 1730-1733.
32. W.-J. Ong, L.-L. Tan, Y. H. Ng, S.-T. Yong and S.-P. Chai, *Chem. Rev.*, 2016, **116**, 7159-7329.
33. J. Liu, H. Wang and M. Antonietti, *Chem. Soc. Rev.*, 2016, **45**, 2308-2326.
34. Y. Shiraishi, S. Kanazawa, Y. Sugano, D. Tsukamoto, H. Sakamoto, S. Ichikawa and T. Hirai, *ACS Catal.*, 2014, **4**, 774-780.
35. V. S. Kale, U. Sim, J. Yang, K. Jin, S. I. Chae, W. J. Chang, A. K. Sinha, H. Ha, C.-C. Hwang, J. An, H.-K. Hong, Z. Lee, K. T. Nam and T. Hyeon, *Small*, 2017, **13**.
36. M. Zhu, S. Kim, L. Mao, M. Fujitsuka, J. Zhang, X. Wang and T. Majima, *J. Am. Chem. Soc.*, 2017, **139**, 13234-13242.
37. L. Lin, W. Ren, C. Wang, A. M. Asiri, J. Zhang and X. Wang, *Appl. Catal. B Environ.*, 2018, **231**, 234-241.
38. Y. Zhao, Z. Liu, W. Chu, L. Song, Z. Zhang, D. Yu, Y. Tian, S. Xie and L. Sun, *Adv. Mater.*, 2008, **20**, 1777-1781.
39. C. Wang, H. Daimon, T. Onodera, T. Koda and S. Sun, *Angew. Chem. Int. Ed.*, 2008, **47**, 3588-3591.
40. Y.-Y. Cai, X.-H. Li, Y.-N. Zhang, X. Wei, K.-X. Wang and J.-S. Chen, *Angew. Chem. Int. Ed.*, 2013, **52**, 11822-11825.
41. H. Su, K.-X. Zhang, B. Zhang, H.-H. Wang, Q.-Y. Yu, X.-H. Li, M. Antonietti and J.-S. Chen, *J. Am. Chem. Soc.*, 2017, **139**, 811-818.
42. J. Y. Park, L. R. Baker and G. A. Somorjai, *Chem. Rev.*, 2015, **115**, 2781-2817.
- S. M. Kim, S. J. Lee, S. H. Kim, S. Kwon, K. J. Yee, H. Song, G. A. Somorjai and J. Y. Park, *Nano Lett.*, 2013, **13**, 1352-1358.
44. W. Iqbal, B. Yang, X. Zhao, M. Rauf, M. Waqas, Y. Gong, J. Zhang and Y. Mao, *Catal. Sci. Technol.*, 2018, **8**, 4576-4599.
45. Y. Zhang, X. Weng, H. Li, H. Li, M. Wei, J. Xiao, Z. Liu, M. Chen, Q. Fu and X. Bao, *Nano Lett.*, 2015, **15**, 3616-3623.
46. O. Björneholm, A. Nilsson, H. Tillborg, P. Bennich, A. Sandell, B. Hernnäs, C. Puglia and N. Mårtensson, *Surf. Sci.*, 1994, **315**, L983-L989.
47. R. Vakili, E. K. Gibson, S. Chansai, S. Xu, N. Al-Janabi, P. P. Wells, C. Hardacre, A. Walton and X. Fan, *Chemcatchem*, 2018, **10**, 4238-4242.
48. R. Bliem, J. E. S. van der Hoeven, J. Hulva, J. Pavelec, O. Gamba, P. E. de Jongh, M. Schmid, P. Blaha, U. Diebold and G. S. Parkinson, *Proc. Natl. Acad. Sci.*, 2016, **113**, 8921-8926.
49. L. Xu, X.-C. Xu, L. Ouyang, X.-J. Yang, W. Mao, J. Su and Y.-F. Han, *J. Catal.*, 2012, **287**, 114-123.



A “Mott–Schottky modulated catalysis” on Pt nanoparticles was reported to promote Pt catalysis for CO oxidation.